Excited states and size-dependent electro-optical properties of CdS_xSe_{1-x} quantum dots

Kevin L. Stokes* and Peter D. Persans
Department of Physics, Applied Physics and Astronomy, Rensselaer Polytechnic Institute, Troy, New York 12180
(Received 6 November 1995; revised manuscript received 15 March 1996)

The electric-field response of $CdS_{0.44}Se_{0.56}$ quantum dots in glass is studied as a function of particle size using electroabsorption spectroscopy. Up to six quantum-size levels can be observed in the data. The evolution of the transitions through many particle sizes provides evidence for mixing of the valence bands due to quantum confinement. The electromodulated absorption data were fit with a first-derivative line-shape function to separate the effects of the electric field on the energy level, width, and oscillator strength associated with each electron-hole state. For the lowest excited state in particles with radius R less than the bulk exciton Bohr radius, the size dependence of the field-induced redshift is $\propto R^4$ and the decrease in oscillator strength is $\propto R^6$, consistent with perturbation theory. Although perturbation theory predicts the proper power-law dependence, the magnitude of the response is many times smaller than predicted. The field-induced redshift of the second excited state is found to increase as a function of decreasing particle size with a maximum occurring for particles with radius nearly equal to bulk Bohr exciton radius. [S0163-1829(96)05828-6]

I. INTRODUCTION

Semiconductor particles with diameters on the order of 10 nm or less are small enough to confine the electrons and holes in all three dimensions and are referred to as ''quantum dots.'' The extent to which the carriers are confined depends on the ratio of the particle radius compared to the bulk Bohr exciton radius. Effects of quantum confinement on the electronic and optical properties of these materials are evident in particles whose size is on the order of a few times the Bohr exciton radius and smaller.[1] The confinement of electrons and holes in a semiconductor quantum dot is usually divided into three general size regimes.[2] In the weak confinement regime, the particle radius R is larger than the bulk Bohr exciton radius a_x. In this case the center-of-mass motion of the exciton is quantized. In the intermediate confinement regime $a_e > R > a_h$, where a_e is the Bohr radius of the electron and a_h is the Bohr radius of the hole. Here, the energy of the electron is higher than that of the hole, since the electron is considerably lighter. The electron energies are quantized and the interaction of the electron and hole is taken into account by assuming that the hole moves in an average potential created by the rapidly moving electron.[2] In the strong confinement regime the particle is smaller than either a_e or a_h, the Coulomb interaction is neglected, and the electrons and holes are independently quantized.[2]

The study of the optical and electro-optical properties of semiconductor quantum dots is driven by potential device applications. Quantum confinement transforms the energy band structure of the bulk semiconductor into a series of discrete transitions. This is interesting for electro-optical devices since the energetic positions of these transitions can be manipulated by an external electric field. Since electroabsorption is a quadratic electro-optical effect, it has the potential, at least, for application as wavelength selective, polarization-insensitive amplitude modulators. A variety of devices have already been fabricated with one-dimensionally confined semiconductor structures, the so-called ''quantum wells.''[3] The electroabsorption mechanism in quantum wells is referred to as the quantum-confined Stark effect (QCSE).[4,5] Two quantum well devices that operate on the QCSE are the bistable self-electro-optic effect device[6] (SEED) and the optical quantum well modulator.[7] Theoretically, the three-dimensionally confined quantum dots offer the advantage of lower switching energy over quantum wells. Near an electron-hole transition energy, the predicted change in the absorption coefficient per unit mass per unit applied field is much larger in a quantum dot than in a quantum well.[8] However, these predictions neglect the effects of surfaces and defects, which could degrade actual device performance.

Electroabsorption (EA) spectroscopy is used to measure the electric-field effects on the electronic states in a quantum dot. This type of modulation spectroscopy is useful for analyzing electronic properties since the detailed shape and magnitude of the electric-field-induced changes in the absorption spectra depend not only on the extent of confinement but also on the nature and symmetry of the excited state. Electroabsorption selects states that are the most sensitive to electric field and also allows the observation of dipole-forbidden transitions. States are clearly evident in electroabsorption spectra that are not apparent in linear absorption. The quantification of the electric-field sensitivity provides information about the symmetry and charge distribution of the electronic wave functions.

Electroabsorption spectroscopy has been used by many research groups to investigate the properties of II-VI semiconductor quantum dots.[9–18] There are several proposed mechanisms for the field modulation of the absorption: Stark shift,[10,11,15] Franz-Keldysh oscillations,[13] oscillator strength changes,[10,15] lifetime changes due to tunneling,[9,19] or broadening due to the Stark effect on an ensemble of dipole excited states.[20] The detailed understanding of the electro-optical properties of these systems requires the correct interpretation of the EA spectra. The magnitude of the electro-optical effect is a strong function of particle size. Intuitively, the largest electro-optical response should be found in the largest particles since these wave functions are

more easily polarized, provided the exciton is prevented from ionizing by the quantum confinement. This is seen qualitatively from experiment although the functional dependence and overall magnitude are smaller than expected.[18,19] We now examine the electro-optical response of semiconductor quantum dots over a wide range of particle sizes. We deconvolve the spectra to experimentally quantify the particle size dependence of the field-induced redshift, broadening, and change in oscillator strength of the two lowest excited states.

The lowest excited state in semiconductor quantum dots and its dependence on particle size have been extensively studied.[1,21,22] The theoretical interpretation usually assumes that a single valence band is being quantized. However, three distinct valence bands exist in most semiconductors of interest.[23] The spherical symmetry of the quantum dots introduces an orbital angular momentum that couples with the intrinsic $j=3/2$ momentum of the valence-band Bloch functions.[24] The valence bands can no longer be considered independently. Good quantum numbers are the square and z component of the total angular momentum, $\mathbf{I}=\mathbf{L}+\mathbf{J}$, where $\mathbf{L}$ is the angular momentum of envelope function and $\mathbf{J}$ is the valence-band angular momentum. As a result, the hole wave functions contain linear combinations of l and $l+2$ envelope functions. Additionally, all three valence-band Bloch functions must be included to match the boundary conditions at the quantum dot–host interface.[25–27]

There are many theories for the calculation of the energies and optical dipole moments of the higher excited states that account for the confinement-induced valence-band mixing; some include the effects of finite confinement potential, nonparabolic bands, and electron-hole correlation.[25,26,28–31] However, there are relatively few experimental studies of the higher excited states to compare with theory. The size-dependent hole spectrum of CdSe quantum dots was characterized by two separate research groups. Ekimov *et al.* used standard linear absorption spectroscopy and located the excited states in the relatively featureless spectra by taking numerical derivatives of the data.[26] The results were compared to the theory that they developed.[26] Norris *et al.* studied the excited states in CdSe quantum dots using two different size-selective optical spectroscopies: Nanosecond pump-probe spectroscopy and photoluminescence excitation spectroscopy.[27] The nature of the hole energy state spectrum depends heavily on the effective-mass parameters of the bulk crystal. For example, the ground-state (lowest-energy) hole wave function for CdSe and other semiconductors with a large spin-orbit splitting energy has total angular momentum $I=3/2$ and is therefore a mixture of the two uppermost bulk valence bands and contains a combination of the S and D envelope wave functions.[25,26,28] In contrast, CdS has a small spin-orbit spitting and its ground-state hole wave function is predicted to have P symmetry.[29] It follows, therefore, that excited states in CdS_xSe_{1-x} quantum dots, with $x>0$, should now be investigated.

This paper focuses on two issues concerning semiconductor quantum dots: The nature of the excited electron-hole states and the magnitude of the electro-optical response. Both issues are addressed with data obtained from a detailed electroabsorption study involving several particle sizes of $CdS_{0.44}Se_{0.56}$ quantum dots in glass. The particle sizes range from $2a_x$ (intermediate confinement) to $0.5a_x$ (strong confinement), where $a_x \approx 3.5$ nm is the bulk Bohr exciton radius for this semiconductor composition. We have included samples with particle sizes ranging from the intermediate to strong confinement regimes because this allows us to observe the evolution from a bulklike valence-band structure to the more complicated quantum-confined band structure. Sample preparation and electroabsorption experimental methods are described in Sec. II. The results are given in Sec. III. The energetic positions of the excited-state transitions are easily located in the EA data. As many as six transitions can be observed in some spectra. Also included in Sec. III is a description of the spectral deconvolution, which is necessary so that the effects of the electric field on the electronic states can be quantified. In Sec. IV, we discuss the results of Sec. III in terms of the available theories with emphasis on the identification of the excited-state transitions and the magnitude of the electro-optical response. Finally, a summary and conclusion are given in Sec. V.

II. EXPERIMENT

The samples were prepared by thermal treatment of commercially available Schott RG630 filter glass. Raman spectra show that the particle composition is unaffected by this treatment.[32] Details of the sample preparation and characterization are published elsewhere.[33] Ten samples were studied with average particle radius ranging from 6.2 to 1.7 nm.[18] Direct particle-size measurements of five samples were made by transmission electron microscopy (TEM). We estimated the particle size of the remaining samples by assuming that the energy shift in the lowest excited state is given by $E_x=E_g+\hbar^2\pi^2/2\mu R^2$, where E_g is the bulk band gap, μ is an effective-mass parameter, and R is the particle radius.[1,2] The particle radii from TEM (samples RG-1, RG-3, RG-6, and RG-7) were used to obtain a reasonable fit with the function above using $E_g=1.93$ eV and $\mu=0.15m_e$. The TEM measurement of RG-8 was excluded because the particle size was below the resolution limit of the electron microscope.

The samples were polished to a thickness of 70–120 μm using standard 600-grit wet/dry sandpaper followed by chemomechanical polish. The polished samples were sandwiched between two indium-tin-oxide coated glass slides, which served as electrodes. A thin piece of transparent plastic film along with a small amount of an insulating, index-matching fluid (Fluorinert[34] FC-70) were also included to avoid unwanted signal from modulation of the air space between the sample and the electrode.

The electroabsorption experiment is the same as in Ref. 18. The probe beam was derived from a 150-W Xe arc lamp passed through a 0.25-m monochromator; the spectral resolution was about 20 meV at $\lambda=600$ nm. The transmitted light was detected with a Si photodiode with no reverse bias. The photodiode current was amplified with a basic operational-amplifier current-to-voltage circuit, which had a gain of $10^6\ \Omega$. The output of this preamp was connected to both a Stanford Research Systems SR530 lock-in amplifier to monitor the modulated (ac) light intensity and a Keithley 197 digital multimeter to monitor the dc transmitted light intensity. A variable neutral density filter placed in front of the sample kept the dc intensity level constant to $\pm 5\%$. A

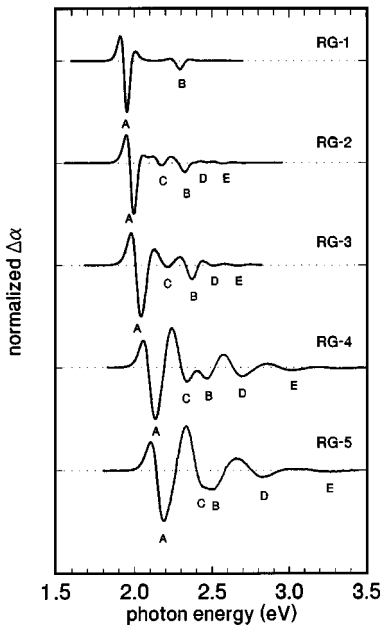

FIG. 1. Electroabsorption spectra of the $CdS_{0.44}Se_{0.56}$ quantum dots in glass for a field strength of 100 kV/cm. The spectra are normalized so that the magnitude of the lowest-energy structure is constant. Actual maximum magnitudes are (in cm^{-1}) 0.17 (RG-1), 0.077 (RG-2), 0.019 (RG-3), 0.021 (RG-4), and 0.015 (RG-5). Each label appears near a $-\Delta\alpha$ peak.

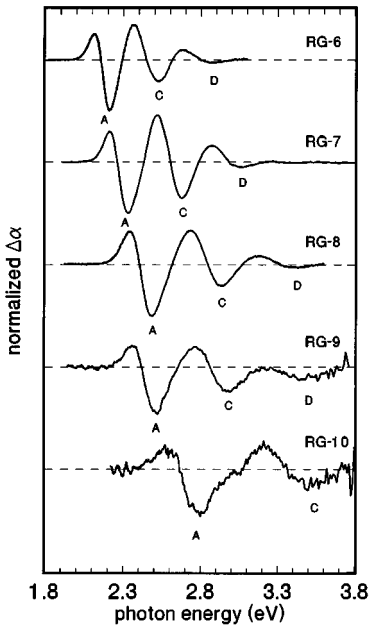

FIG. 2. Electroabsorption spectra of the $CdS_{0.44}Se_{0.56}$ quantum dots in glass for a field strength of 100 kV/cm. The spectra are normalized so that the magnitude of the lowest-energy structure is constant. Actual maximum magnitudes are (in cm^{-1}) 0.019 (RG-6), 0.0088 (RG-7), 0.0033 (RG-8), 0.0020 (RG-9), and 0.00035 (RG-10). Each label appears near a $-\Delta\alpha$ peak.

sinusoidal voltage of about 1-kV peak was applied across the electrodes resulting in an external electric field of about 100 kV/cm. The frequency of the applied voltage was 1.75 kHz and the modulation signal was recovered at twice the modulation frequency (3.5 kHz) by the lock-in amplifier. The experiment was performed at room temperature.

III. RESULTS

A. Electroabsorption spectra

Electroabsorption spectra for all ten $CdS_{0.44}Se_{0.56}$ samples are shown in Figs. 1 and 2. The electric-field-induced change in absorption is obtained simply from

$$\Delta\alpha = \left(-\frac{1}{d}\right)\frac{\Delta T}{T}, \tag{1}$$

where ΔT is the modulated (ac) transmissivity, T is the steady-state (dc) transmissivity, and d is the sample thickness. Because of the variation in thickness between samples, the applied field was different for different samples. In order to make quantitative comparisons between spectra, all the spectra were normalized to a reference electric field strength of 100 kV/cm.

Spectral features (zero crossings, positions, and relative magnitude of maxima and minima) are independent of field strength up to 100 kV/cm. The signal magnitude scales with the square of applied field. When the modulation signal is proportional to the square of the perturbation, as in this case, the signal is recovered from the lock-in at twice the modulation frequency and 90° out of phase with the reference signal as shown below. The modulation signal V_{ac} is proportional to the electric field squared, $|\mathbf{F}|^2$, or

$$V_{ac} \propto |F_0 \sin(\omega t)|^2 \propto \frac{F_0^2}{2}[1+\sin(2\omega t - \pi/2)]. \tag{2}$$

We also monitored the signal at the fundamental modulation frequency and determined that there was no linear component of the electro-optical response.

Standard linear absorption data for these samples are given in Ref. 18. The characteristic blueshift of the lowest-energy transition is easily seen. However, the peaks are broad and, at most, only three peaks can be observed in the data. In the electroabsorption spectra, any $-\Delta\alpha$ peak indicates the existence of a separate electron-hole transition, assuming that the electric field cannot cause a blueshift or narrowing of the absorption band. This assumption is justified since the energy of the system must decrease in the presence of an electric field.[4] The fact that each transition has (at most) a single $-\Delta\alpha$ minimum can be seen by examining the spectral line-shape function described in Sec. III B below. For purposes of discussion, we have labeled the spectral features in Figs. 1 and 2 as A, B, C, D, and E. A sixth feature appears in sample RG-4 at 3.35 eV (see Fig. 1) but it is not labeled since a similar feature could not be positively identified in any other sample.

As the particle size is decreased, the position of the lowest spectral feature (A) shifts upwards in energy from 1.95 eV in sample RG-1 (Fig. 1) to 2.70 eV in sample RG-10 (Fig. 2). Also notice that the width of the spectral features increases with increasing energy. This inhomogeneous broadening is due to the distribution of particle sizes and shapes. Sample RG-1 contains the largest quantum dots with 6.2-nm average

radius. Only two sharp modulation features are evident in this spectrum, A and B, centered at 1.95 and 2.29 eV, respectively. These spectral structures have been previously identified as transitions from the highest valence band and the spin-orbit split-off valence band.[17] This spectrum is different from the spectra of the smaller particles, which show additional transitions. Also, this EA spectrum is not bulklike since no Franz-Keldysh oscillations are present. We believe that the absence of additional peaks is the result of this particular sized quantum dot in which the exciton binding energy, confinement energy, and electric-field energy are of the same order.

In the smaller particle-sized samples (RG-2 through RG-10) the additional spectral features are denoted by the letters C, D, and E. The electronic transition labeled C appears first in sample RG-2. As the particle size decreases, this feature grows until it appears to merge with the spin-orbit feature B (see Fig. 1, sample RG-5). For the samples containing the smallest particles (RG-9 and RG-10) again only two spectral features can be positively identified. Notice, too, that the spectra in Figs. 1 and 2 are normalized. The actual magnitude of the electro-optical response decreases by a factor of ~ 500 from the largest particles (RG-1) to the smallest (RG-10).

B. Line-shape analysis

In order to quantify electric-field response of the electronic transitions in the electroabsorption spectra, we fit the data with a first-derivative line-shape function.[18,35] In a bulk semiconductor, the change in the absorption coefficient induced by the electric field is proportional to the third derivative of the zero-field absorption (excluding excitonic effects).[36,37] However, since the electrons are confined inside the quantum dot, they cannot accelerate in the electric field. The electric-field-induced change in the dielectric function is proportional to the total first derivative of the unperturbed dielectric function with respect to the electric field[35,38]

$$\Delta\epsilon = \frac{\partial\epsilon}{\partial f_{n,n'}}\Delta f_{n,n'} + \frac{\partial\epsilon}{\partial E_{n,n'}}\Delta E_{n,n'} + \frac{\partial\epsilon}{\partial\Gamma_{n,n'}}\Delta\Gamma_{n,n'}, \quad (3)$$

where $f_{n,n'}$ is the oscillator strength, $E_{n,n'}$ is the transition energy, and $\Gamma_{n,n'}$ is the linewidth of the electron-hole transition labeled by the subscripts n and n', which indicate the possible quantum numbers of the electron and hole, respectively. The effects of the electric field on the oscillator strength, transition energy, and width are determined from the coefficients $\Delta f_{n,n'}$, $\Delta E_{n,n'}$, and $\Delta\Gamma_{n,n'}$. The contributions of the individual terms in Eq. (3) to the total line-shape function are shown graphically in Ref. 39. For electroabsorption, the perturbation of the real part of the dielectric function is neglected.[40] The imaginary part of the dielectric function is, of course, proportional to the absorption coefficient. We assume that the absorption band for each electron-hole transition (n, n') can be written as a Gaussian function, which is appropriate for inhomogeneously broadened excitonic absorption.[9,41,42] The EA spectrum is the sum of the derivative functions from the individual electron-hole transitions.

The commercially available software, PEAKFIT,[43] was used to fit the first derivative line-shape function to the data.

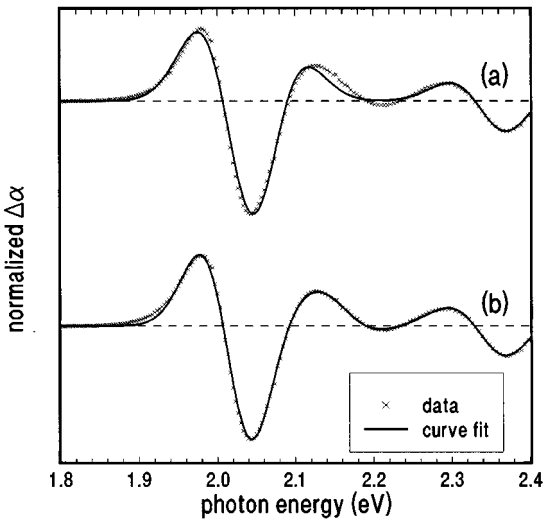

FIG. 3. Electroabsorption and curve fit for sample RG-3 using (a) only two electronic transitions and (b) three electronic transitions, corresponding to the three $-\Delta\alpha$ peaks.

The line-shape function was input into PEAKFIT as a user-defined function. PEAKFIT allows the initial parameter values to be selected with the aid of a graphic interface and solves for the parameters using the Marquardt-Levenberg nonlinear least-squares algorithm.[43] Unfortunately, curve fitting is as much an art as a science. The spectral peaks overlap and the final parameter values depend to some extent on the initial values. To minimize the ambiguity in the parameter values, we used the smallest number of parameters necessary to satisfactorily fit each peak. In most cases, for the peaks labeled A and C, including the broadening parameter $\Delta\Gamma$ did not statistically improve the quality of the fit. For the spin-orbit peak (B), the energy shift parameter ΔE was not needed. The quality of the curve fits was determined by the correlation coefficient. All curve fits had correlation coefficient $r \geqslant 99\%$ except samples RG-9 and RG-10, which had $r = 97\%$ and $r = 90\%$, respectively. We point out that a single spectrum cannot be considered in isolation. An important part of the curve fitting procedure is the ability to track the evolution of the peaks through many particle sizes.

Linear optical absorption data were used to convert the parameter values into physical quantities.[40] The quantities ΔE, $\Delta\Gamma$, and $\Delta f/f$ are independent of both the oscillator strength and width of the absorption band and are most closely associated with properties of a single quantum dot.

Typical curve fitting examples are given in Figs. 3(a) and 3(b) for sample RG-3. In Fig. 3(a), only two transitions are used in an attempt to fit the spectrum. Clearly, the fit is unsatisfactory in the 2.15–2.30-eV region. This shows explicitly that there is no possible way to account for the small $-\Delta\alpha$ peak considering only the fundamental (A) and spin-orbit (B) transitions. The appropriate curve fit is given in Fig. 3(b), which uses three transitions corresponding to each $-\Delta\alpha$ peak.

The curve-fitting procedure allows the quantitative determination of the field-induced modulation mechanisms through the three parameters describing the redshift, broadening, and change in oscillator strength. For the larger particle sizes, RG-1, RG-2, and RG-3, spectral feature A is best

fit using a redshift in exciton energy, broadening, and a decrease in oscillator strength. The ratio of broadening to redshift decreases from 2 for sample RG-1 to 0.6 for sample RG-3. For samples RG-4 through RG-10, the broadening parameter is zero. The spin-orbit feature (B) is dominated by broadening with some decrease in the oscillator strength.

In all samples where it appears, we find that feature C is best modeled with a redshift and an *increase* in the oscillator strength. This fact is used to identify this higher-energy spectral feature in samples RG-5, RG-6, RG-7, RG-8, RG-9, and RG-10. There is some question about the identity of feature C in samples RG-6 and RG-7 since this feature appears at an energy approximately 0.33 eV above the lowest-energy transition and could be confused with the spin-orbit transition. We identify this as spectral feature C since it can only be modeled assuming an increase in oscillator strength. This can be seen qualitatively from Fig. 2. Consider the $+,-,+\Delta\alpha$ lobe structure of the lowest-energy transition. For all these samples the $+\Delta\alpha$ lobe on the high-energy side of the transition is larger (in magnitude) than the corresponding $+\Delta\alpha$ lobe on the low-energy side. Compare this with the EA spectra for RG-1, RG-2, and RG-3 in Fig. 1 where the $+\Delta\alpha$ feature on the high-energy side is smaller than the lower-energy $+\Delta\alpha$ lobe. Only an increase in oscillator strength (corresponding to a $+\Delta\alpha$) of the second, higher-energy transition can satisfactorily account for this feature in those spectra in which these features overlap.

C. Error in the parameter estimates

The two important aspects of the electroabsorption data are the locations (in energy) of the spectral features and the magnitude of the spectra as a response to electric field. The error in the energetic locations of the spectral features (peaks and zero crossings) is a function of the resolution of the monochromator and the signal-to-noise ratio and is less than 1 meV. However, the line-shape analysis shows that the electronic transition energy may not strictly coincide with either a $-\Delta\alpha$ peak or a zero crossing. For this reason, the upper limit on the error in the electronic transition energy obtained from the curve-fitting procedure is on the order of $\Gamma/2$, where Γ is the (Gaussian) transition width.

The magnitude of the electric-field-induced redshift, broadening, and change in oscillator strength are subject to two sources of uncertainty: uncertainty in the internal electric-field strength and uncertainty in the curve-fitting parameters. The applied electric field is estimated by measuring the voltage applied across the electrodes and dividing by the thickness of the sample structure, which consists of the glass sample plus two sheets of plastic film. (There is a negligible potential drop due to the finite resistance of the electrodes.) Note that the applied electric field is different than the electric field inside the semiconductor particle, which is estimated below. All the results shown are normalized to an *applied* electric-field strength of 100 kV/cm.

The absolute magnitude of the electric field inside the semiconductor quantum dot is estimated as follows. The voltage V is applied across the glass sample, with static dielectric constant $\epsilon_{\rm gl}\approx 5$ and thickness $d_{\rm gl}$, which is surrounded by two layers of plastic film, each with dielectric constant $\epsilon_f\approx 2$ and thickness d_f. Since the dielectric constant of the plastic wrap is lower than the dielectric constant of the glass-semiconductor composite sample, a nontrivial amount of the electric field is dropped across the plastic film. From basic electrostatics, the field across the glass sample is

$$F_{\rm gl}=\frac{\epsilon_f[2(d_f/d_{\rm gl})+1]}{2\epsilon_{\rm gl}(d_f/d_{\rm gl})+\epsilon_f}F_0, \tag{4}$$

where $F_0=V/(2d_f+d_{\rm gl})$ is the applied electric-field magnitude. The sample thickness is nominally 100 μm and each layer of plastic film is about 12 μm so that 75% of the applied field is dropped across the glass sample.[40]

The difference in the dielectric constants of the glass host material and the semiconductor particles must also be considered. Inside the semiconductor quantum dot, the field is obtained from[44]

$$F_{\rm QD}=\frac{\epsilon_{\rm gl}}{g\epsilon_{\rm QD}+(1-g)\epsilon_{\rm gl}}F_{\rm gl}, \tag{5}$$

where $\epsilon_{\rm QD}=9.0$ is the static dielectric constant of the $CdS_{0.44}Se_{0.56}$ semiconductor particle and g is a geometrical depolarization factor equal to 1/3 for a sphere. Therefore the electric field inside the particle is 80% of the field across the glass or roughly 60% of the applied field.

A large part of the uncertainty in the parameter estimates originates from the uncertainty in d_f and $d_{\rm gl}$. The sample thickness is measured with a standard mechanical micrometer and is uniform to less than 5 μm or 5%. The actual thickness of the two layers of plastic film can vary up to ± 10 μm depending on how tightly the sample sandwich is squeezed together. This results in an error in the estimation of the applied electric field of 15%. The error in the normalization of the spectra to the same electric-field strength is 30%, since this normalization depends on the field squared. This, then, is the dominant source of error in the relative magnitude of the field-dependent parameter estimates (redshift, broadening, and change in oscillator strength). The second source of error comes from the inherent uncertainty in the parameters due to curve fitting. The error in the parameter values obtained from the curve-fitting procedure is estimated from the 90% confidence limits and depends on the both the standard deviation of the experimental data and the amount of peak overlap. For the samples with the largest particle sizes, this error may be as low as 3% for the lowest-energy transition. However, for the smallest particles this error can be as large as 50% for the relatively small spectral features, which have a significant amount of overlap as in sample RG-5 (see Fig. 1).

IV. DISCUSSION

A. Hole energy spectrum

The excited-state transition energies from the electroabsorption data are shown in Fig. 4. The excited-state energies were obtained from location of the $-\Delta\alpha$ minima in the EA data. Since the higher excited states are plotted as differences from the lowest excited state, these data should be insensitive to EA line shape. No single simple theory is available to explain the data shown in Fig. 4 since the particle sizes extend over two quantum-size regimes, intermediate and strong

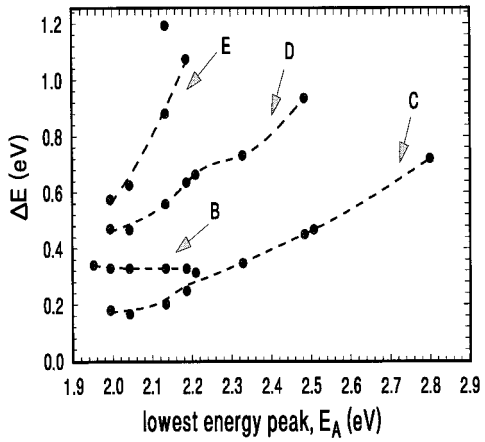

FIG. 4. Electron-hole transition energies from the electroabsorption data. The transition energies are plotted relative to the lowest excited state, E_A, identified as $1S_{3/2}$-$1S_e$. The dashed lines connect similar transitions, for example, all the third excited states are connected, and are intended as visual guides. The letters (A, B, C, D, and E) label the transitions as in Figs. 1 and 2.

confinement. The band gap for a bulk material of this composition, $CdS_{0.44}Se_{0.56}$ is about 1.93 eV. Therefore, the kinetic energy due to quantum confinement is experimentally given by $E_{QC}=E_A-1.93$ eV. Based on simple theory,[1,21] a particle with radius $R=a_x$ has confinement energy approximately equal to 0.3 eV. Roughly, then, the samples with E_{QC} less than 0.3 eV (or $E_A<2.23$ eV) are in the intermediate confinement regime and samples with $E_{QC}>0.3$ eV are in the strong confinement regime. Of course there is no clear distinction between the confinement regimes and evolution of wave functions and energy levels from one regime to the other needs to be addressed theoretically.

We will discuss the results in terms of the confinement-induced valence-band mixing theory using the notation of Ekimov *et al.*[26] to label the excited states. The electron states are simply given by nL_e, where n is the number of the level in energy ordering and L is the angular momentum of the envelope function in atomic notation, $S,P,D,F\ldots$ for $l=0,1,2,3\ldots$ The subscript e is a redundant reminder that this is an electron state. The hole states are given by nL_I, where n is the number of the level of a given symmetry (as with the electron states), L is the minimum orbital angular momentum of the envelop function included in the hole wave function (the other is $L+2$), and I is the total angular momentum of the state. For example, the highest hole state wave function for CdSe and other semiconductor quantum dots with a large (bulk) spin-orbit splitting energy has $I=3/2$ and is a combination of the S and D orbital wave functions.[25,26,28]

The lowest-energy transition (A) in all our spectra is identified as the $1S_{3/2}$-$1S_e$ excitation. The shift of peak B is nearly constant with respect to the $1S_{3/2}$-$1S_e$ (A) for the larger particles, $E_A<2.25$ eV. This splitting is $E_B-E_A=0.33\pm0.01$ eV. This means that either the quantization of the electron is dominating over that of the hole (as in the intermediate confinement regime) or the two valence bands are being independently quantized at the same rate. The latter explanation requires that the effective mass of the holes is approximately the same for each of the valence bands. In either case, spectral feature B is identified as the transition from the spin-orbit split-off valence band and the $1S_e$ conduction band. This identification is consistent with the expected splitting for material of this composition.[33,45] We have confirmed that the splitting of this feature shifts properly with particle composition for large particles. At energy $E_A\approx2.25$ eV, transitions B and C overlap. At energies $E_A>2.25$ eV, only transition C is observed.

An interesting consequence of the confinement-induced valence-band mixing is the ''disappearance'' of the transition from the spin-orbit valence-band hole state to the lowest electronic state. This should occur for materials with a large spin-orbit splitting and is implicit in the calculations of Ekimov *et al.* for CdSe.[26] When the confinement energy is on the order of the spin-orbit splitting energy, there is significant mixing of all three valence bands for states with $I=3/2$ and lowest-energy state has S symmetry. However, for $I=1/2$, even parity states, the lowest state has P symmetry and does not contain the heavy-hole valence band. It is this state that converges to the top of the spin-orbit valence band as $R\rightarrow\infty$. This explains the constant (bulklike) shift of the spin-orbit-derived transition relative to the $1S_{3/2}$-$1S_e$ for the larger particles. As the confinement energy approaches the spin-orbit splitting energy ($\Delta_{SO}=0.33$ eV), the state that evolves primarily from the spin-orbit valence band takes on its P-like character. Therefore, in the smaller quantum dots this state is not optically connected to the $1S_e$ state. This is seen to occur at about $E_A=2.25$ eV.

The identification of the transition labeled C relies on its response to electric field. Recall that transition C is characterized by an increase in oscillator strength with applied field. The probability of dipole allowed transitions in the semiconductor quantum dot is determined by the square of the overlap integral of the electron and hole wave functions.[2,26,30] An increase in oscillator strength (with applied electric field) can occur as a result of a previously forbidden transition becoming allowed. The electric field does couple states with different angular symmetry so that transitions with $\Delta l=\pm1$ become possible. However, the C transition appears in the linear absorption data, indicating that it is a dipole allowed transition or that the quantum dot is not perfectly spherical.

Valence-band mixing also modifies the radial quantum number selection rule so that transitions from nL hole states to mL electron states become allowed from $n\neq m$ provided the angular quantum number is conserved.[26,30] Transitions from a hole state that has a bimodal charge distribution ($n=2$) to an electron state with a unimodal charge distribution ($m=1$) is allowed. This means that a field-induced redshift can be accompanied by an increase in the overall electron-hole overlap. For this reason the C peak is identified as the $2S_{3/2}$-$1S_e$ transition.

At this time we have not attempted to identify transitions D, E, and F of Fig. 4. Comparisons of the quantum-size levels with the calculations for CdSe (Refs. 25 and 26) and CdS (Ref. 29) reported in the literature can only be made qualitatively. Correct identification of the transitions requires calculations of the hole energy levels for our ternary compound. We are also unable to draw any quantitative conclu-

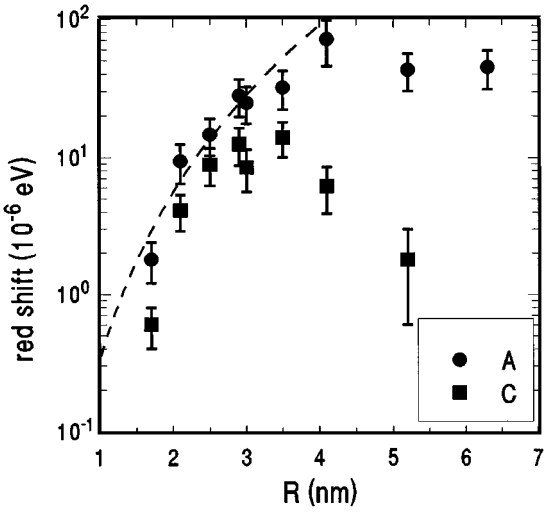

FIG. 5. Electric field-induced redshift for the first (lowest-energy) excited state (A) and second excited state (C) as a function of particle size. The dashed line is a fit to Eq. (6) for state A and is proportional to R^4.

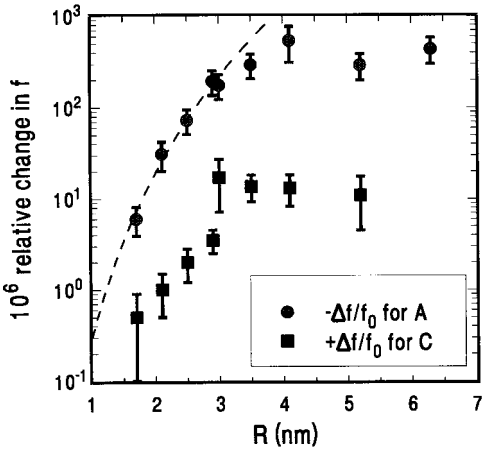

FIG. 6. Electric field-induced change in oscillator strength for the first (lowest-energy) excited state (A) and second excited state (C) as a function of particle size. The dashed line is a fit to Eq. (7) for state A and is proportional to R^6. Note that the change in oscillator strength for state C is positive, indicating an increase in oscillator strength with applied field.

sions about the magnitude of the electric-field-induced modulation mechanisms since these peaks are small and broad.

We observe that transitions that involve the $1S_e$ electronic transition are the most sensitive to electric field. Of course, the higher-energy wave functions are much less sensitive to the electric field since they reside higher in the quantum well. Also, there are strictly no bound states in the presence of an electric field since the electron can always tunnel to a lower energy level. In the limit that the spacing between electronic levels was on the order of the electric-field energy, the discrete levels would appear to be a continuum in the presence of the field. However this would also be true for the hole and this effect is not observed for the hole states.

B. Electro-optic response

The measured size dependence of the electro-optic response of the $CdS_{0.44}Se_{0.56}$ quantum dots in glass is shown in Figs. 5 and 6. The data are the results of the deconvolution procedure described in Sec. III B. Due to the inherent uncertainties in determining the field-dependent parameter values, the data are plotted on a semilogarithmic graph to emphasize that we should interpret the data in terms of trends and orders of magnitude. The error in the parameter values is discussed in Sec. III C. The data shown are for the first two excited-state transitions, labeled A and C (Figs. 1 and 2). Sample RG-9 was not included for the following reasons. This sample was broken while being polished and the only piece usable for the electroabsorption measurements was very small (only a few millimeters square) and about 30 μm thick. It was impossible to ensure that all of the probe light was going through the sample to reach the detector. Also, the small thickness meant that estimation of the electric field was subject to greater error. While this has no effect on the line shape, the uncertainty in the magnitude of the electro-optical response was so large that the sample was not useful for this analysis.

Before examining the data more closely, we briefly review the electric-field effects on the electronic transitions in a semiconductor quantum dot. In a bulk semiconductor, the effect of the electric field is well documented.[36,46,47] Primarily, the effects are a finite, exponentially decreasing absorption tail below the band gap and pseudo-periodic oscillations above the band gap (Franz-Keldysh oscillations). In semiconductors with a prominent exciton peak, the effect of the electric field is to ionize the exciton and therefore broaden the peak due to the decreased lifetime. In quantum dots, the exciton cannot ionize since it is confined by the quantum dot boundary; in fact the exciton is stable up to many times the classical ionization field.[11,25] The main effect of the electric field is to lower the electron-hole transition energy. The energy of the system is lowered due to an increased separation of the electron and hole (polarization). The effect is referred to as the quantum-confined Stark effect since the field-induced separation is quadratic in the electric field and occurs whether the electron and hole are bound by their mutual Coulomb interaction (as in the weak or intermediate confinement limit) or bound by the walls of the quantum well (as in the strong confinement limit). In addition to a redshift of the transition energy, the oscillator strength and selection rules are modified in the presence of the electric field. For the lowest-energy transition, $1S_{3/2}$-$1S_e$, the spatial separation of the electron and hole results in a decrease of the electron-hole overlap and hence the oscillator strength. The electric field also couples states with orbital angular momentum l and $l\pm1$ so that transitions between states with S and P symmetry are weakly allowed. Miller *et al.* have derived a general sum rule, which states that the integrated change in absorption (electric field on minus field off) is zero.[8,48] This means that a decrease in oscillator strength of allowed transitions is compensated by the growth of forbidden transitions.

In general, calculations of the electric field effect on the energies and wave functions of quantum-confined electrons and holes must be done numerically. Perturbation theory cannot be used in the weak and intermediate confinement

regimes since the confinement energy, Coulomb interaction energy, and applied electric field energy on all of the same order. No analytic wave function that solves the boundary conditions and includes electron-hole correlation is possible. For this reason, variational methods have been used.[19] Closed-form approximations are possible in the strong-confinement limit where the Coulomb interaction is neglected. The field-induced energy shift and change in oscillator strength for the lowest-energy transition calculated from second-order perturbation theory are given by[49]

$$\Delta E_{1S_h\text{-}1S_e} = -0.090M\frac{2e^2F^2}{\hbar^2\pi^2}R^4 \tag{6}$$

and

$$\frac{\Delta f_{1S_h\text{-}1S_e}}{f_0} = -0.080M^2\frac{4e^2F^2}{\hbar^4\pi^4}R^6, \tag{7}$$

where $M=m_e+m_h$ is the total electron-hole effective mass and f_0 is the zero-field oscillator strength.

The size dependence of the field-induced redshift for the lowest excited state is shown in Fig. 5. Recall that these data represent the intrinsic electric field response of a single quantum dot; the parameter values are independent of both the oscillator strength and the width of the absorption band. In the strong-confinement limit, the Stark shift is given by Eq. (6). This model was compared to the data in Fig. 5. Using the electric field as an adjustable parameter, this simple perturbation-theory result fits the smaller particle sizes (less than 3 nm) reasonably with an electric field of 13 kV/cm. This is about 5 times smaller than the estimated field inside the quantum dots of 60 kV/cm. The larger particle sizes show a much weaker electric-field response dependence on particle radius; the dependence is approximately proportional to R. The redshift for the second excited state, C, shows an interesting behavior (Fig. 5). The redshift increases with decreasing particle size for the particles with average radius $R \geqslant 3$ nm and then decreases with decreasing particle size for particles with $R<3$ nm. The rate of decrease is approximately the same as for the redshift of the A transition.

The change in oscillator strength induced by the electric field as a function of particle size is shown in Fig. 6. The data were compared to the prediction of second-order perturbation theory, Eq. (7). As for the redshift, the electric-field magnitude was used as an adjustable parameter. An electric field of 7 kV/cm seems to match the small particle sizes. Note that the sign of the change in oscillator strength is different for transitions A and C in Fig. 6.

The redshift of the lowest-energy exciton peak that we observe is much smaller than the shift of the exciton in GaAs-based quantum-well device structures. Miller *et al.* observed shifts of $\sim$ 5 meV for an electric field strength of 60 kV/cm in multiple $GaAs/Al_xGa_{1-x}As$ quantum-well structures.[4,5] These wells consist of alternating 10-nm layers of GaAs and $Al_xGa_{1-x}As$. The bulk Bohr exciton radius for GaAs is about 15 nm. It is difficult to compare the amount of confinement in the quantum wells to quantum dots because the quantum wells are finite wells and the confinement is only in one direction. In any case, the largest redshift that we observed was 0.05 meV for the $R=6.2$ nm particles with an estimated internal electric field of 60 kV/cm. Theoretically, the electric-field-induced energy shifts for the quantum dot should be identical to those in a quantum well of the same thickness (if the Coulomb interaction is neglected).[8] Nomura and Kobayashi point out that the Coulomb interaction is more important in quantum dots than in quantum wells since the ratio of Coulomb interaction energy to confinement energy is higher in quantum dots.[19] Based on calculations, they conclude that the Coulomb interaction cannot be neglected even for particles as small as $a_x/3$. However, including the Coulomb effect in their variational calculation failed to account for the small field-induced energy shifts that they observed in their quantum-dot system.[9,19]

As stated above the small-particle electric field response indicates that the electric field inside the quantum dot is 5–7 times smaller than is estimated from the applied field. Charges may be present on the quantum-dot surface. If these charges exist in a surface band they may be very efficient at screening the electric field. (The surface band structure has been calculated by Wang and Duke[50]). Alternatively, the lowest excited state may be a mixture of an S-like interior state and intrinsic surface states as suggested by Bawendi *et al.*[51] This would result in a state that has charge distribution maxima at the center and surface of the quantum dot making it much less sensitive to electric field.

Field-induced broadening was found to be a significant effect in the A transition only for the three largest particle sizes, RG-1, RG-2, and RG-3. Therefore, we cannot draw any conclusions about the size dependence of this effect. We think that it is unlikely that any three-lobed structure in the EA spectrum of the lowest excited state is broadening caused by field ionization of the exciton, although this has been suggested by some researchers.[19] The applied electric fields are actually on the order of or less than the classical ionization fields for bulk CdS and CdSe, $F=140$ and 60 kV/cm, respectively.[47] The confinement is known to increase the binding energy of the exciton, thereby allowing it to survive in fields many times the bulk ionization field.[11,25] Field-induced broadening is not important for smaller particles. However, broadening does seem to be the dominant electro-optical effect for the states originating from the spin-orbit split valence band. This indicates that the hole can tunnel from the spin-orbit band to a lower valence band in the presence of the electric field.

It has been argued that the dominant electroabsorption mechanism for the lowest excited state is broadening, based on comparisons of EA spectra with second derivatives of linear absorption.[16] This is explained by assuming that the lowest electronic state in CdSe quantum dots has a significant dipolar character due to wave-function mixing with the surface state. The dominant electric-field effect on an ensemble of randomly oriented dipoles is to effectively broaden the transition and is, in fact, quadratic in the electric field.[16,20] However, this theory fails to account for any redistribution of oscillator strength in the presence of the applied field. Norris *et al.* have suggested that in the limit of broad absorption linewidths, larger than both the field-induced shifts and separation between states, a redshift of the transition energy along with the appearance of forbidden transitions can appear to be a single broadened transition.[27] The

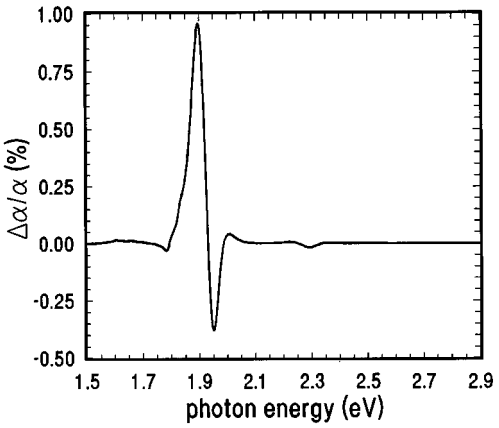

FIG. 7. Normalized change in absorption for sample RG-1.

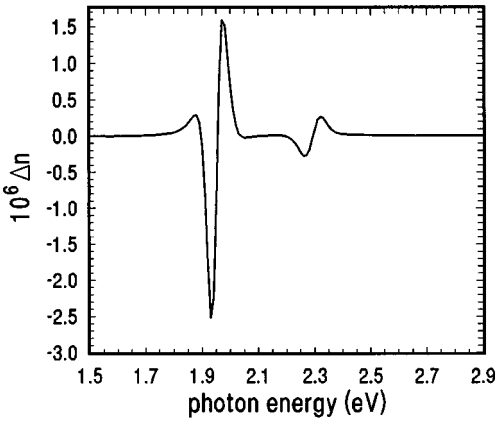

FIG. 8. Change in the real part of the index of refraction induced by the electric field for sample RG-1.

EA line shape will then resemble the second derivative of the linear absorption with respect to energy.

C. Implications for device applications

The fact that the magnitude of the field response is much smaller (25–50 times) than the theoretical prediction is troubling. Either the current theory of the nature of the excited states is quantitatively incorrect, or there is an important screening mechanism that we have overlooked. In this section we discuss the consequences of the experimental results for potential device applications.

Three fundamental design considerations for devices based on the QCSE are the modulation depth (on/off intensity ratio), the accompanying change in the real part of the index of refraction and the bandwidth.[52] The intrinsic bandwidth is a function of the response time of the electron-hole pairs and cannot be addressed with this experiment. A figure of merit for the strength of the electro-optic effect is given by $\Delta\alpha/\alpha$. A graph of $\Delta\alpha/\alpha$ for sample RG-1 is shown in Fig. 7. Recall that sample RG-1 contains the largest particles, $R=6.2$ nm or about twice the Bohr exciton radius. Almost all the electro-optic response is concentrated in the lowest-energy transition. Many more electronic states exist but they are not affected by the field. The maximum fractional change in absorption is only about 1% and this is at least an order of magnitude below what is necessary for practical applications.

A problem inherent in electroabsorption modulators is frequency chirping due to the change in the real part of the index of refraction.[52] Figure 8 shows the change in index of refraction for sample RG-1 calculated from the Kramers-Kronig relation

$$\Delta n(\omega)=\mathrm{Pr}\frac{c}{\pi}\int_0^\infty \frac{\Delta\alpha(\omega')}{\omega'^2-\omega^2}d\omega', \tag{8}$$

where Pr denotes the principal part of the integral. Comparing Fig. 8 with Fig. 7 shows that the maximum change in absorption occurs near a zero change in the index of refraction, which is ideal characteristic for a modulation device based on electroabsorption.

The electro-optical response of semiconductor quantum dots requires further study. The R^4 dependence of the redshift for the small particles suggests that larger particles are more useful for practical applications. There must be enough quantum confinement to stabilize the exciton in the electric field and concentrate the oscillator strength into discrete lines, but not enough confinement to produce confinement-induced valence-band mixing effects. The disadvantage of intermediate confinement is that the excited states are closer together. However, since the higher excited states are not sensitive to field, as in sample RG-1, this confinement regime offers the most promise.

V. CONCLUSION

Electroabsorption was used as a sensitive probe of the electronic transitions in $CdS_{0.44}Se_{0.56}$ quantum dots in glass. Ten samples with average particle radius ranging from $R=6.2$ nm to $R\approx 1.7$ nm were studied. These particle sizes range from the intermediate to strong confinement regimes. Only two electro-optically active transitions are observed in the largest particles. Up to six quantum-size levels can be observed in the intermediate-sized particles. The evolution of the transitions through many particle sizes provides evidence for mixing of valence bands due to quantum confinement. The electronic transition originating from the spin-orbit split-off valence band is seen in the larger particle sizes, but disappears when the size is reduced below the bulk exciton Bohr radius.

The electroabsorption spectra were used to quantify the electric-field effects on the absorption and index of refraction of the quantum dots, particularly near the lowest-energy excitonic transition. Transitions involving electron-hole envelope functions with S-like symmetry are the most sensitive to electric field. The electroabsorption data were fit with a first-derivative line-shape function to separate the effects of the electric field on the energy level, width, and oscillator strength associated with each electron-hole state. For the smaller particles, $R<a_x=3.5$ nm, the redshift of the excitonic transition is found to be proportional to R^4 and the change in oscillator strength is proportional to R^6, in agree-

ment with perturbation theory. The larger particles, $R > a_x$, have a much weaker dependence on particle size. The field-induced redshift in the large particles is at least an order of magnitude smaller than the electric-field induced shift observed in GaAs-based quantum wells with similar confinement, that is, the well width compared to a_x. Electric-field-induced broadening of the transition width was found to be negligible.

*Present address: Materials Science and Technology Division, Naval Research Laboratory, Washington, DC 20375-5000.

[1] L. Brus, J. Chem. Phys. **80**, 4403 (1984).
[2] A. Efros and A. Efros, Fiz. Tekh. Poluprovodn. **16**, 1209 (1982) [Sov. Phys. Semicond. **16**, 772 (1982)].
[3] P. Bhattacharya and K. Dutta, Annu. Rev. Mat. Sci. **23**, 79 (1993).
[4] D. Miller *et al.*, Phys. Rev. B **32**, 1043 (1985).
[5] D. Miller *et al.*, Phys. Rev. Lett. **53**, 2173 (1984).
[6] D. Miller *et al.*, Appl. Phys. Lett. **45**, 13 (1984).
[7] T. Wood *et al.*, IEEE J. Quantum Electron. **21**, 117 (1985).
[8] D. Miller, D. Chemla, and S. Schmitt-Rink, Appl. Phys. Lett. **52**, 2154 (1988).
[9] S. Nomura and T. Kobayashi, Solid State Commun. **73**, 425 (1990).
[10] F. Hache, D. Ricard, and C. Flytzanis, Appl. Phys. Lett. **55**, 1504 (1989).
[11] A. Ekimov, A. Efros, T. Shubina, and A. Skvotsov, J. Lumin. **46**, 97 (1990).
[12] H. Rossmann, S. Schulzgen, F. Henneberger, and M. Muller, Phys. Status Solidi B **159**, 287 (1990).
[13] D. Cotter, H. Girdlestone, and K. Moulding, Appl. Phys. Lett. **58**, 1455 (1991).
[14] V. Esch *et al.*, Phys. Rev. B **42**, 7450 (1990).
[15] V. Esch *et al.*, Int. J. Nonlin. Opt. Phys. **1**, 25 (1992).
[16] V. Colvin, K. Cunningham, and A. Alivisatos, J. Chem. Phys. **101**, 7122 (1994).
[17] G. Mei, S. Carpenter, L. Felton, and P. Persans, J. Opt. Soc. Am. B **9**, 1394 (1992).
[18] K. Stokes, H. Yukselici, and P. Persans, Solid State Commun. **92**, 195 (1994).
[19] S. Nomura and T. Kobayashi, Solid State Commun. **74**, 1153 (1990).
[20] V. Colvin and A. Alivisatos, J. Chem. Phys. **97**, 730 (1992).
[21] L. Banyai and S. Koch, *Semiconductor Quantum Dots* (World Scientific, Singapore, 1993).
[22] M. Bawendi, M. Steigerwald, and L. Brus, Annu. Rev. Phys. Chem. **41**, 477 (1990).
[23] M. Cohen and J. Chelikowsky, *Electronic Structure and Optical Properties of Semiconductors*, 2nd ed. (Springer-Verlag, New York, 1989).
[24] K. Vahala and P. Sercel, Phys. Rev. Lett. **65**, 239 (1990).
[25] F. Henneberger and J. Puls, in *Optics of Semiconductor Nanostructures*, edited by F. Henneberger, S. Schmitt-Rink, and E. Gobel (Akademie-Verlag, Berlin, 1993), p. 497.
[26] A. Ekimov *et al.*, J. Opt. Soc. Am. B **10**, 100 (1993).
[27] D. Norris, A. Sacra, C. Murray, and M. Bawendi, Phys. Rev. Lett. **72**, 2612 (1994).
[28] J. Xia, Phys. Rev. B **40**, 8500 (1989).
[29] G. Grigoryan, E. Kazaryan, A. Efros, and T. Yazeva, Fiz. Tverd. Tela (Leningrad) **32**, 1772 (1990) [Sov. Phys. Solid State **32**, 1031 (1990)].
[30] J. Pan, Phys. Rev. B **46**, 4009 (1992).
[31] S. Koch, Y. Hu, B. Fluegel, and N. Peyghambarian, J. Cryst. Growth **117**, 592 (1992).
[32] A. Tu and P. Persans, Appl. Phys. Lett. **58**, 1506 (1991).
[33] G. Mei, Ph.D. thesis, Rensselaer Polytechnic Institute, Troy, NY, 1992.
[34] Fluorinert is a trade name for a transparent liquid mixture of completely fluorinated aliphatic compounds and is available from SIGMA Chemicals, St. Louis, MO. The type FC-70 mixture has an index of refraction of 1.303 at 25 °C which closely matches the index of the plastic film.
[35] O. Glembocki and B. Shanabrook, in *The Spectroscopy of Semiconductors*, edited by D. Seiler and C. Littler, Semiconductors and Semimetals Vol. 36 (Academic, Boston, MA, 1992), p. 222.
[36] M. Cardona, *Modulation Spectroscopy* (Academic, New York, 1969).
[37] D. Aspnes, Surf. Sci. **37**, 418 (1973).
[38] R. Enderlein, D. Jiang, and Y. Tang, Phys. Status Solidi B **145**, 167 (1988).
[39] Y. Hirayama, W.-Y. Choi, L. Peng, and C. Fonstad, J. Appl. Phys. **74**, 570 (1993).
[40] K. Stokes, Ph.D. thesis, Rensselaer Polytechnic Institute, Troy, NY, 1995.
[41] Y. Huang, H. Qiang, and F. Pollack, J. Appl. Phys. **70**, 3808 (1991).
[42] D. Chemla *et al.*, IEEE J. Quantum Electron. **20**, 265 (1984).
[43] PEAKFIT - A Reference Manual, Jandel Scientific, San Rafael, CA, 1991.
[44] L. Genzel and T. Martin, Surf. Sci. **34**, 33 (1973).
[45] S. Nomura and T. Kobayashi, Solid State Commun. **78**, 677 (1991).
[46] B. Snavely, Phys. Rev. **167**, 730 (1968).
[47] D. Blossey and P. Handler, in *Modulation Techniques*, edited by R. Willardson and A. Beer, Semiconductors and Semimetals Vol. 9 (Academic, New York, 1972), p. 257.
[48] D. Miller, J. Weiner, and D. Chemla, IEEE J. Quantum Electron. **22**, 1816 (1986).
[49] F. Henneberger *et al.*, Semicond. Sci. Technol. **16**, A41 (1991).
[50] Y. Wang and C. Duke, Phys. Rev. B **37**, 6417 (1988).
[51] M. Bawendi, P. Carroll, W. Wilson, and L. Brus, J. Chem. Phys. **96**, 946 (1992).
[52] Y. Kan, H. Masamichi, and I. Suemune, IEEE J. Quantum Electron. **23**, 2167 (1987).